Selective Variant Growth of Coherent Precipitate under External Constraints

D.Y. Li and L.Q. Chen*
Department of Materials Science and Engineering
The Pennsylvania State University, State College, PA 16802, USA

(Submitted 27 January 1998; in revised form 15 July 1998)

An anisotropic distribution of coherent precipitate variants may result in anisotropic behavior of a two-phase material. The distribution of the coherent precipitate variants can be controlled using constrained aging. This article reports our experimental and computational studies of the stress effect on the spatial arrangement of coherent precipitate variants. The research demonstrates that the anisotropic elastic coupling between applied stress/strain and the local strain caused by the lattice mismatch between different phases makes the growth of differently oriented phase variants selective. $Ti_{11}Ni_{14}$ precipitation in a Ti-51.5at.%Ni alloy was investigated as a particular example. It was demonstrated that the constrained aging strongly affected the distribution of $Ti_{11}Ni_{14}$ precipitate variants. The resulting selective variant growth of $Ti_{11}Ni_{14}$ precipitates can be predicted based on the symmetry analysis and the elastic energy calculation.

Introduction

It is well known that coherent precipitates in a two-phase material strongly affect mechanical and tribological properties of the material (Ref 1-5). These properties may be further improved if precipitate variants are spatially arranged in a particular way. This is best demonstrated by the two-way shape memory effect of a nickel-rich TiNi alloy that experienced constrained aging, which produced an anisotropic distribution of coherent $Ti_{11}Ni_{14}$ precipitate variants (Ref 6). The two-way shape memory effect relies on a long-range internal stress field caused by a parallel alignment of the coherent lenticular $Ti_{11}Ni_{14}$ precipitates in this alloy. The long-range internal stress field controls the "path" of reversible martensitic transformations, and thus results in a superior two-way shape memory effect, called all-round shape memory effect (Ref 6).

A coherent precipitate phase usually has a number of variants oriented in different directions (Ref 7-9) if the precipitate phase has a lower symmetry than the matrix. During aging without any external constraint, all the precipitate variants may grow with the same probability and arrange themselves in a self-accommodative way to minimize the strain energy. However, if an external constraint, for example, an applied stress, is applied during aging, the variants could be distributed anisotropically (Ref 6, 8).

In order to improve our understanding of the constraint effect on the distribution of coherent precipitate variants and to identify the factors that control the selection of preferred variants, systematic investigation on the selective variant growth was carried out. This article reports our research, combining theoretical, modeling, and experimental studies, on the selective variant growth of $Ti_{11}Ni_{14}$ precipitates in a constraint-aged Ti-51.5at.%Ni shape memory alloy.

*Present address: Department of Chemical and Materials Engineering, University of Alberta, Edmonton, Alberta, Canada T6G2G6

Theoretical Analysis

Determination of the Variant Number of a Coherent Precipitate Phase

The variant number of a coherent precipitate phase can be determined by analyzing the symmetry-breaking change during precipitation by decomposing the space group of the parent phase into the coset of the space group of the precipitate (Ref 7). Suppose the space group of the parent phase is G_0 and the space group of precipitate is G_1, the coset decomposition is represented as:

$$G_0 = N_{01}G_1 = \{N_1, N_2, ..., N_m\}G_1 \quad \text{(Eq 1)}$$

where $N_1, N_2, ..., N_m$ are elements of the space group G_0, but they do not belong to G_1. The number of these elements gives the number of different orientation variants, which is equal to m.

If a stress is applied during the precipitation process, the number of variants is also influenced by the symmetry of the stress "environment." In this case, the coset decomposition is performed on the intersection of G_0 and the space group of the stress constraint, (g), that is:

$$H_0 = G_0 \cap (g) = N^S_{01}\, G_1 = \{N^S_1, N^S_2, \ldots, N^S_l\}G_1 \quad \text{(Eq 2)}$$

where $N^S_1, N^S_2, \ldots, N^S_l$ are the elements belonging to both the space groups of the parent phase and the stress constraint. H_0 is the space group of isoprobability of nucleation of the product phase, which usually has fewer elements than G_0. As a result, the number of the variants is reduced because $l < m$.

TiNi alloy has a *B*2 structure (a_o = 3.01 Å) (Ref 10), and its space group is *Pm*3*m* (Ref 11). The $Ti_{11}Ni_{14}$ precipitate has a rhombohedral structure (a_o = 6.72 Å, γ = 113.9°), and its space group is $R\bar{3}$ (Ref 12, 13). The corresponding crystallographic relation between the precipitate and the parent phase is $(111)_{Ti_{11}Ni_{14}} // \{111\}_{B2}$ (Ref 6). The number of variants can be determined by decomposing the space group of the parent phase into the coset of the precipitate space group, that is:

$$G_0 = Pm3m = N_{01}G_1 = (h_1 + h_2 + h_3 + h_4 + h_{13} + h_{14} + h_{15} + h_{16})R_{\bar{3}\,[111]} \quad \text{(Eq 3)}$$

where h_i (i = 1, 2, ..., 16) are the following operation elements:

h_1, identity transformation
h_2, 180° rotation about $(100)_{B2}$
h_3, 180° rotation about $(010)_{B2}$
h_4, 180° rotation about $(001)_{B2}$
h_{13}, 180° rotation about $(\bar{1}10)_{B2}$
h_{14}, 90° rotation about $(001)_{B2}$
h_{15}, 270° rotation about $(001)_{B2}$
h_{16}, 180° rotation about $(110)_{B2}$

One may see that the $Pm\bar{3}m$ group can be decomposed into eight cosets of the $R_{\bar{3}}$ group, thus resulting in eight $Ti_{11}Ni_{14}$ phase variants. The eight symmetry operations, h_i, are equivalent to rotating the [111] axis of a $Ti_{11}Ni_{14}$ variant to $[111]_{B2}$, $[\bar{1}\bar{1}\bar{1}]_{B2}$, $[\bar{1}11]_{B2}$, $[1\bar{1}\bar{1}]_{B2}$, $[1\bar{1}1]_{B2}$, $[\bar{1}\bar{1}1]_{B2}$, $[11\bar{1}]_{B2}$, and $[\bar{1}\bar{1}1]_{B2}$, respectively. The eight $Ti_{11}Ni_{14}$ variants have already been observed experimentally (Ref 12) and found to be distributed in a self-accommodative way corresponding to the minimum elastic energy. However, when the aging is under a constraint, the self-accommodative distribution can be broken, and the variant growth becomes selective. In principle, those variants, whose growth minimizes the strain energy of the system, have a higher probability to grow.

The Elastic Energy of a Coherent Precipitate

The first calculation of the strain energy of a coherent precipitate was made in 1957 by Eshelby (Ref 14, 15), who derived equations to calculate the elastic strain of an ellipsoidal inclusion in an isotropic matrix based on the assumption that both phases have the same elastic moduli. Eshelby's theory was modified, extended, and developed later by many researchers (Ref 16-21) to make it suitable for the anisotropic elasticity case. A general elastic theory of a coherent two-phase system with arbitrary morphology in the homogeneous modulus approximation was proposed in 1967 by Khachaturyan (Ref 22). In Khachaturyan's theory, the exact equation for strain energy and the Fourier transform of elastic displacement in an arbitrary two-phase coherent mixture were derived. This theory was later extended to arbitrary coherent mixtures comprising inclusions formed by crystal lattice rearrangements of different types (Ref 23), using which, one may obtain all the results of Eshelby's theory. Khachaturyan's theory has recently been extended to the elastically inhomogeneous case (Ref 24).

According to Khachaturyan (Ref 9), in the case of homogeneous elastic modulus, the stress-free transformation strain, $\varepsilon^o_{ij}(\vec{r})$, is primarily dependent on the shape function, $\theta(\vec{r})$, which describes the shape of the precipitate:

$$\varepsilon^o_{ij}(\vec{r}) = \varepsilon^o_{ij}\theta(\vec{r}) \quad \text{(Eq 4)}$$

where ε^o_{ij} corresponds to stress-free strain for the precipitate when $\theta(\vec{r}) = 1$. The final elastic energy expression of a coherent precipitate is expressed as:

$$E_{el} = \frac{V}{2} C_{ijkl}\bar{\varepsilon}_{ij}\bar{\varepsilon}_{kl} - V_p C_{ijkl}\bar{\varepsilon}_{ij}\varepsilon^o_{kl} + \frac{V_p}{2} C_{ijkl}\varepsilon^o_{ij}\varepsilon^o_{kl} - \frac{1}{2}\int \frac{d^3k}{(2\pi)^3}(n_i\sigma^o_{ij}\Omega_{jk}(\vec{n})\sigma^o_{kl}n_l)|\theta(\vec{k})|^2 \quad \text{(Eq 5)}$$

where V_p and V are the volume of the precipitate and the total volume of the system, respectively. C_{ijkl} is the elastic constant, and $\sigma^o_{ij} = C_{ijkl}\varepsilon^o_{kl}$. $\vec{n} = \vec{k}/k$ is a unit vector in the reciprocal space, and n_i is the ith component of $\vec{n}$. $\Omega_{jk}(\vec{n})$ is a Green function matrix reciprocal to $\Omega^{-1}_{jk}(\vec{n}) = n_i C_{ijkl} n_l$. $\theta(\vec{k})$ is the Fourier transform of the shape function $\theta(\vec{r})$ whose value equals the unity when $\vec{r}$ is within the precipitate and equals zero when outside the precipitate.

When a precipitate grows under an applied strain or stress, its coherent strain energy is changed. There are two types of constraints (Ref 25). One is the *strain constraint,* in which the system's boundary is fixed after applying an external force to the system, followed by the precipitation process. Under such a condition, the system is subjected to a constant external strain. The second type of constraint, called *stress constraint,* is to apply a constant stress on the system without fixing the boundary of the system.

In the strain-constraint case, the total elastic energy is obtained by replacing the homogeneous strain in Eq 5 by the applied homogeneous strain, that is, $\bar{\varepsilon}_{ij} = \varepsilon^a_{ij}$:

$$E^{\varepsilon}_{el} = \frac{V}{2} C_{ijkl}\bar{\varepsilon}^a_{ij}\bar{\varepsilon}^a_{kl} + \frac{V_p}{2} C_{ijkl}\varepsilon^o_{ij}\varepsilon^o_{kl} - \frac{1}{2}\int \frac{d^3k}{(2\pi)^3}[n_i\,\sigma^o_{ij}\Omega_{jk}(\vec{n})\sigma^o_{kl}n_l]|\theta(\vec{k})|^2 - V_p C_{ijkl}\varepsilon^a_{ij}\varepsilon^o_{kl} \quad \text{(Eq 6)}$$

The last term in Eq 6 represents the coupling between the external strain and the coherent strain caused by the precipitate. The strain-constraint condition was used to investigate the effect of external constraint on the selective variant growth in the present study. As for the stress-constraint condition, the effect of constraint stress is similar to that of the strain-constraint

effect, although the expression of the strain energy is slightly different from Eq 6 (Ref 25).

Strain Energy Variation of a $Ti_{11}Ni_{14}$ Precipitate Caused by External Strain

The coherent strain of a $Ti_{11}Ni_{14}$ precipitate comes from the lattice mismatch between the precipitate and the matrix. Experiments have demonstrated that a $Ti_{11}Ni_{14}$ precipitate has a lenticular (Ref 6) shape. This has also been illustrated by recent simulation studies (Ref 25). For a coherent disc-like precipitate, the strain caused by the lattice mismatch reaches its maximum in the direction perpendicular to the precipitate disc (Ref 26). In the case of a $Ti_{11}Ni_{14}$ precipitate, the maximum mismatch occurs along the normal to the precipitate disc (i.e., $\langle 111 \rangle_{B2}$). The eigenstrain matrix of the $Ti_{11}Ni_{14}$ precipitate, when expressed in a coordinate frame with its three axes respectively parallel to $[1\bar{1}0]_{B2}$, $[11\bar{2}]_{B2}$, and $[111]_{B2}$, has the following value:

$$(\varepsilon^{o}_{ij}) = \begin{pmatrix} 0.014 & 0 & 0 \\ 0 & 0.014 & 0 \\ 0 & 0 & -0.029 \end{pmatrix} \div \qquad \text{(Eq 7)}$$

From the eigenstrain matrix, one may see that this eigenstrain causes a tensile strain perpendicular to the $Ti_{11}Ni_{14}$ precipitate disc, and minor compressive strain parallel to the disc, when the $Ti_{11}Ni_{14}$ precipitate is formed in a TiNi matrix.

The elastic energy of $Ti_{11}Ni_{14}$ precipitate was calculated using Khachaturyan's elastic theory. The calculation indicates that a $Ti_{11}Ni_{14}$ precipitate variant whose diameter equals 0.2 μm has its elastic energy equal to 3.08×10^{-8} ergs. For this calculation, the x, y, and z axes of the chosen coordinate frame are respectively parallel to $[1\bar{1}0]_{B2}$, $[11\bar{2}]_{B2}$, and $[111]_{B2}$ of TiNi ($B2$) lattice, in which the $Ti_{11}Ni_{14}$ precipitate disc has its normal parallel to z axis. Elastic constants of the TiNi matrix and the $Ti_{11}Ni_{14}$ precipitate phase were assumed to be the same and had the following values: $C_{11} = 1.62 \times 10^{11}$ Pa, $C_{12} = 1.29 \times 10^{11}$ Pa, and $C_{44} = 0.34 \times 10^{11}$ Pa (Ref 27). Since the given elastic constants are effective only in the coordinate frame (x'-y'-z') whose three axes are parallel to $[100]_{B2}$, $[010]_{B2}$, and $[001]_{B2}$, the elastic constants were converted into ones which were effective in the variant coordinate frame (x-y-z), using the tensor transformation law (Ref 28):

$$C_{ijkl} = S_{ii'} S_{jj'} S_{kk'} S_{ll'} C_{i'j'k'l'} \qquad \text{(Eq 8)}$$

where $S_{ii'}$ is the coordinate transformation matrix that relates the x'-y'-z' coordinate frame to x-y-z coordinate frame.

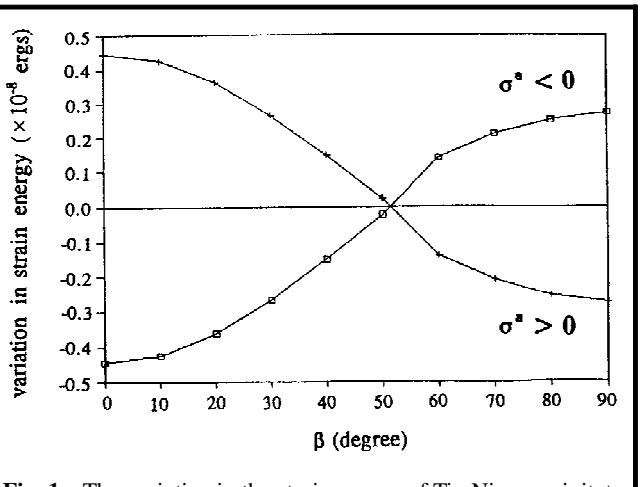

Fig. 1 The variation in the strain energy of $Ti_{11}Ni_{14}$ precipitate caused by the applied load ($\sigma^a = \pm 10$ MPa).

When an external stress is applied, the internal strain is modified with a change in the strain energy barrier to growth of the precipitate. The following calculation has illustrated respective effects of a tensile strain and a compressive strain on the elastic energy of a $Ti_{11}Ni_{14}$ precipitate variant. The external strain was applied in the x-z plane and was at an angle, β, to the z axis, where the z axis is parallel to the normal of the $Ti_{11}Ni_{14}$ disc and the x axis is in the disc plane. Results of the strain energy calculation are given in Fig. 1, which represents the coupling energy, $E^{int} = -V_p C_{ijkl} \varepsilon^a_{ij} \varepsilon^o_{kl}$, between the applied strain and the coherent strain with respect to β. From Fig. 1, one may see that the strain energy of a precipitate variant varies with the direction of applied strain.

As mentioned earlier, $Ti_{11}Ni_{14}$ precipitates were assumed to have the same elastic modulus as that of the TiNi matrix. This assumption simplifies the strain energy analysis. However, in the case of an inhomogeneous modulus, the present analysis is valid, and the strain energy expressions may become similar to those obtained in the homogeneous modulus case by introducing some eigenstrains ε^{**}_{ij} to model the inhomogeneity by the equivalent inclusions with the additional eigenstrains ε^{**}_{ij} (Ref 29).

Prediction of Variant Selection of $Ti_{11}Ni_{14}$ Precipitate under Applied Strains

As demonstrated above, the local strain of each precipitate variant is changed by an applied strain or stress, depending on both the variant orientation and the applied load. Some of the variants are favored to grow, but the others are not. The external constraint, therefore, reduces the number of variants, leading to the selective variant growth.

A pole projection method was proposed to predict the selective variant growth under external constraint. As discussed, the growth of a variant is determined by the coupling of the applied stress/strain and the eigenstrain. If the applying direction of an external stress and $\langle 111 \rangle_{Ti_{11}Ni_{14}}$ axes of $Ti_{11}Ni_{14}$ variants are represented as poles and marked in a pole projection, one may draw a critical contour of $E^{int} = 0$ around each variant pole as shown in Fig. 2. In this figure, the solid and dashed lines are parts of the $E^{int} = 0$ contours that are respectively on outward and inward halves of the reference sphere, which is used for the pole projection. Each contour separates the pole figure into two parts. When falling into one part, the applied stress favors (or opposes) the growth of the variant, while it opposes (or favors) the growth of other variants.

In order to obtain the critical contour around a $Ti_{11}Ni_{14}$ variant, the constraint strain caused by an initially applied stress was first converted into ε^a_{ij}, which were represented in the variant coordinate frame of the variant. E^{int} was then calculated, and the critical contour for the precipitate variant was thus ob-

tained by finding those angles that correspond to $E^{int} = -V_p C_{ijkl} \varepsilon^a_{ij} \varepsilon^o_{kl} = 0$. $Ti_{11}Ni_{14}$ precipitate has eight variants whose $(111)_{Ti_{11}Ni_{14}}$ are respectively parallel to eight equivalent $\{111\}_{B2}$ planes. We may draw the critical contours for four variants, and the rest can be determined by a mirror symmetry operation. For example, if $(111)_{Ti_{11}Ni_{14}} \| (111)_{B2}$ variants are favored to grow, the growth of $(\bar{1}\bar{1}\bar{1})_{Ti_{11}Ni_{14}} \| (\bar{1}\bar{1}\bar{1})_{B2}$ variants is also favored.

Figure 2 illustrates such a $(001)_{B2}$ pole projection for analyzing the $Ti_{11}Ni_{14}$ precipitation. If a compressive stress is within the zone of a specific variant, which is bounded by the critical contour, the stress will favor the growth of the variant; if the stress is tensile, however, it will oppose this precipitate variant. The situation is reversed when the stress pole is outside the zone. In general, the closer a compressive stress pole is to the variant pole, the more favored the variant is; whereas in the case of a tensile stress, the farther apart the stress pole is from the variant pole ($\beta \leq 90°$), the more favored the variant. It should be noted that the selective variant growth depends on the magnitude of the applied constraint as well as the chemical driving force for the reaction. Our limited experiments and simulation showed that the selective variant growth was induced by a stress in the range from 20 to 80 MPa. Further study is necessary to find out the entire effective range of the applied constraint for selective variant growth and its correlation with the chemical driving force.

One may see that there are some overlapped areas in the pole figure. In principle, the preferred variant is determined by the angle between the stress pole and each of the $\{111\}_{Ti_{11}Ni_{14}} \| \{111\}_{B2}$ poles. In the case of a compressive stress, the smaller the angle between the compressive stress pole and a $Ti_{11}Ni_{14}$ variant pole is, the more easily the variant grows. Therefore, when the compressive stress pole is in an overlapped area, the preferential variant growth may be determined by comparing the angles between the stress pole and each relevant variant pole.

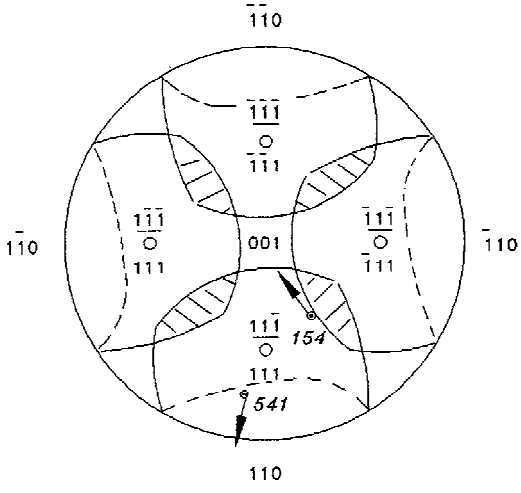

Fig. 2 A (001) pole projection used to analyze the selective $Ti_{11}Ni_{14}$ variant growth. Each zone of a $Ti_{11}Ni_{14}$ variant pole is surrounded by a contour of $E^{int} = 0$. The dashed areas represent the overlapped region of differently oriented variants. The underlined poles point inward.

To illustrate the selective growth under stress constraint, a compressive stress is applied along $[154]_{B2}$ as an example. One may see from the pole projection that the $[154]_{B2}$ ($[\bar{1}\bar{5}\bar{4}]_{B2}$) stress pole is the closest to $[111]_{B2}$ ($[\bar{1}\bar{1}\bar{1}]_{B2}$) and within the zone bounded by $E^{int} = 0$ of this variant pole. As a result, the variants with $(111)_{Ti_{11}Ni_{14}}$ parallel to $(111)_{B2}$ ($(\bar{1}\bar{1}\bar{1})_{B2}$) should precipitate preferentially.

Experimentally Observed and Simulated Morphological Patterns

Experimental Observation

Ti-51.5at.%Ni alloy was prepared in a vacuum consumable arc furnace, followed by homogenization treatment at 900 °C for 5 h, then forged. The specimens cut from the alloy were annealed at 820 °C in an argon atmosphere for 10 min, then aged at 500 °C in an argon atmosphere for 1.5 h. A tensile stress, σ = 38.3 MPa, and a compression stress, σ = –38.6 MPa, were initially applied on two specimens respectively, and the resultant strain, ε^a, was kept unchanged during the aging. A JEM-2000Fx electron microscope (JEOL USA, Inc., Peabody, MA) was employed to investigate the $Ti_{11}Ni_{14}$ precipitation.

Figure 3(a) presents a micrograph of an aged specimen in which one may see differently oriented lenticular $Ti_{11}Ni_{14}$ precipitates with bamboo leaflike cross sections. When the aging was carried out under an external constraint, however, the selective variant growth of $Ti_{11}Ni_{14}$ precipitate occurred and thus resulted in an anisotropic distribution of $Ti_{11}Ni_{14}$ variants. Figure 3(c) illustrates a parallel alignment of $Ti_{11}Ni_{14}$ variants formed under a tensile stress applied horizontally, which was confirmed along $[541]_{B2}$ direction (Ref 30). It has been demonstrated by corresponding TEM diffraction patterns that the precipitates include only two types of variants, whose $[111]_{Ti_{11}Ni_{14}}$ axes are parallel to $[\bar{1}11]_{B2}$ and $[1\bar{1}\bar{1}]_{B2}$ respectively (Ref 30). If marking the tensile stress on the pole projection (Fig. 2), it can be explained why only these two variants grew selectively. As Fig. 2 illustrates, the applied tensile stress pole $[541]_{B2}$ ($[\bar{5}\bar{4}\bar{1}]_{B2}$) is within the zone of the $(111)_{B2}$ ($(\bar{1}\bar{1}\bar{1})_{B2}$) pole, and outside zones of other {111} poles. The stress, therefore, retarded the growth of the $(111)_{Ti_{11}Ni_{14}} \| (111)_{B2}$ ($(\bar{1}\bar{1}\bar{1})_{B2}$) variants. Since the tensile pole is the farthest from the $(\bar{1}11)_{B2}$ ($(1\bar{1}\bar{1})_{B2}$) pole ($\beta \leq 90°$), it favored the growth of $Ti_{11}Ni_{14}$ variants with their $(111)_{Ti_{11}Ni_{14}}$ respectively parallel to the $(111)_{B2}$ and $(\bar{1}\bar{1}\bar{1})_{B2}$ planes. This experimental observation agrees with the theoretical prediction. It should be indicated that $[111]_{Ti_{11}Ni_{14}} \| [111]_{B2}$ and $[111]_{Ti_{11}Ni_{14}} \| [\bar{1}\bar{1}\bar{1}]_{B2}$ variants are not necessarily identical, though they are antiparallel, because they may not have a mirror symmetry. According to the symmetry analysis, there should be eight $Ti_{11}Ni_{14}$ variants, which have been experimentally observed using TEM technique (Ref 12).

Figure 3(b) illustrates the case of a compressive strain constraint applied horizontally, which was along $[154]_{B2}$

($[\overline{154}]_{B2}$). The stress pole was within the zone of $(111)_{B2}$($(\overline{111})_{B2}$) as Fig. 2 illustrates. As predicted, the variants with their $[111]_{Ti_{11}Ni_{14}}$ axes parallel to $[111]_{B2}$ ($[\overline{111}]_{B2}$) precipitated preferentially. The corresponding diffraction patterns (Ref 30) have demonstrated that the observed variants are those predicted by the theory.

Computer Simulation

Computer simulation was also performed to corroborate the theoretical analysis. A diffuse-interface field model was employed. In this model, microstructural development in a coherent two-phase material is described by the temporal evolution of the concentration and structural order parameter field variables. The concentration field distinguishes the compositional difference between the precipitate phase and the matrix, while the structural order parameter field variables distinguish the deference between differently oriented precipitate variants as well as the structural difference between the precipitate phase and the matrix. The driving force for microstructural evolution results from the reduction of the free energy of the system, which includes bulk chemical energy, interphase boundary energy, and the elastic energy. The model has been described in detail elsewhere (Ref 25, 31, 32).

Using this continuum field model, the microstructural evolution in a $Ti_{11}Ni_{14}$-TiNi two-phase alloy under strain constraints was simulated. Figures 4(b) and (c) illustrate the morphological patterns developed under tensile and compressive constraints ($\sigma^a = \pm 80$ MPa) respectively. For a comparison, a morphological pattern formed without external constraint is presented in Fig. 4(a). The microstructures developed from a supersaturated matrix, in which $Ti_{11}Ni_{14}$ particles were randomly embedded at the beginning of the simulation. Under a tensile constraint, those $Ti_{11}Ni_{14}$ variants lying close to the applied tensile stress grew preferentially, while the variants perpendicular to the applied tensile stress were retarded. While the compressive stress has an effect on the variant selection opposite to what the tensile stress has. The results of the

(a) (b) (c)

Fig. 3 **(a)** A microstructure of aged Ti-51.5at.%Ni alloy. **(b)** A parallel alignment of $Ti_{11}Ni_{14}$ variants formed under a compressive stress applied horizontally. **(c)** A parallel alignment of $Ti_{11}Ni_{14}$ variants under a tensile stress applied horizontally.

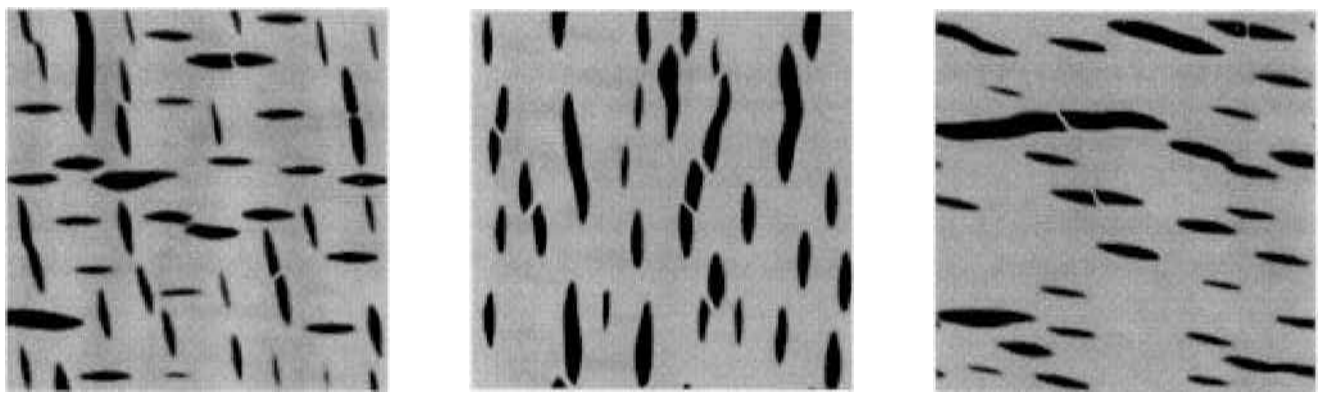

(a) (b) (c)

Fig. 4 Simulated morphological patterns of a $Ti_{11}Ni_{14}$-TiNi alloy formed respectively under the following conditions: **(a)** without external constraint, **(b)** under a compressive stress applied horizontally, and **(c)** under a tensile stress applied horizontally.

simulation studies are consistent with the experimental observation and the theoretical prediction.

Conclusions

A coherent precipitate phase usually has a number of variants oriented in different crystallographic directions. The spatial arrangement of the variants may strongly affect the performance of a two-phase material. The variant number of a coherent precipitate phase depends on the symmetries of involved phases, and it can be determined by decomposing the space group of the parent phase into the coset of the space group of the precipitate phase. However, not all the variants can grow if an external constraint is applied during aging. It was demonstrated that the constrained aging can induce selective variant growth, which can be predicted by analyzing the elastic coupling between the applied stress and the local strain. Coherent $Ti_{11}Ni_{14}$ precipitation in a Ti-51.5at.%Ni alloy during constrained aging was studied, using an approach combining theoretical analysis, experiments, and computer modeling.

Acknowledgment

This work is supported by the Office of Naval Research *Young Investigator Program* under the grant number N-00014-95-1-0577, and the simulation was conducted in the Pittsburgh Supercomputing Center. The experimental work was performed while D.Y. Li was at Department of Materials Physics, University of Science and Technology, Beijing.

Cited References

1. R.E. Smallman, *Modern Physical Metallurgy,* 4th ed., Butterworth & Co., Ltd, London (1985).
2. C.T. Sims and W.C. Hagel, *The Superalloys,* John Wiley & Sons, (1972).
3. J.W. Martin, *Micromechanisms in Particle-Hardened Alloys* (1980).
4. S.M. Copley, *Alloy and Microstructural Design,* J.K. Tian and G.S. Ansell, Ed., Academic Press (1976).
5. D.Y. Li, *Scr. Metall. Mater., 34,* 195 (1995).
6. R. Kainuma, M. Matsumoto, and T. Honma, *Proc. ICOMAT-86,* 717 (1987).
7. R. Portier and D. Gratias, *J. Phys. (France),* Colloque C4, supplement to No. 12, Tome 43, C4-17 (1982).
8. J.W. Stewart, R.C. Thomson, and H.K.D.H. Bhadeshia, *J. Mater. Sci., 29,* 6079-6084 (1994).
9. A.G. Khachaturyan, *Theory of Structural Transformations in Solids,* John Wiley & Sons, New York, (1983).
10. K. Chandra and G.R. Purdy, *J. Appl. Phys., 39,* 2176 (1968).
11. G. Burns and A.M. Glazer, *Space Group for Solid State Scientists,* 2nd ed., Academic Press, Boston (1990).
12. M. Nishida, C.M. Wayman, R. Kainuma, and T. Honma, *Scr. Metall. Mater., 20,* 899 (1986).
13. T. Saburi, S. Nenno, and T. Fukuda, *Proc. XIth Int. Conf. on Electron Microscopy,* Kyoto, 1631 (1986).
14. J.D. Eshelby, *Proc. Roy. Soc., A241,* 376 (1957).
15. J.D. Eshelby, *Proc. Roy. Soc., A252,* 561 (1959).
16. L.J. Walpole, *Proc. Roy. Soc. (A), 300,* 270 (1967).
17. N. Kinoshita and T. Mura, *Phys. Status Solidi (a), 5,* 759 (1971).
18. R.J. Asaro and D.M. Barnett, *J. Mech. Phys. Solids, 23,* 77 (1975).
19. T. Mura, T. Mori, and M. Kato, *J. Mech. Phys. Solids, 24,* 305 (1976).
20. J.K. Lee, D.M. Barnett, and H.I. Aaronson, *Metall. Trans., 8A,* 963 (1977).
21. T. Mori, P.C. Cheng, M. Kato, and T. Mura, *Acta Metall., 26,* 1435 (1978).
22. A.G. Khachaturyan, *Sov. Phys. Solid State, 8,* 2163 (1967).
23. A.G. Khachaturyan and G.A. Shatalov, *Sov. Phys. JETP, 29,* 557 (1969).
24. A.G. Khachaturyan, S. Semenovskaya, and T. Tsakalakos, *Phys. Rev. B, Condens. Matter, 52,* 1 (1995).
25. D.Y. Li and L.Q. Chen, *Acta Mater., 45,* 2435 (1997).
26. D.A. Porter and K.E. Easterling, *Phase Transformations in Metals and Alloys,* Van Nostrand Reinhold (1989).
27. O. Mercier and K.N. Melton, *J. Appl. Phys., 51*(3), 1833 (1980).
28. F.I. Fedorov, *Theory of Elastic Waves in Crystals,* Plenum Press, New York (1968).
29. T. Mura, *Micromechanics of Defects in Solids,* Martinus Nijhoff Publishers, The Hague, The Netherlands, 151 (1982).
30. D.Y. Li and L.Q. Chen, *Acta Mater., 45,* 471 (1997).
31. Y. Wang, L.Q. Chen, and A.G. Khachaturyan, "Modeling of Dynamical Evolution of Micro/Mesoscopic Morphological Patterns in Coherent Phase Transformations," *Computer Simulation in Materials Science, Nano/Meso/Macroscopic Space and Time Scales, NATO Advanced Study Institute Series,* H.O. Kirchner et al., Ed., Kluwer Academic Publishers, Dordrecht, 325 (1996).
32. D.Y. Li and L.Q. Chen, *Acta Mater., 46,* 639, 2573 (1998).